EUROPEAN JOURNAL OF COMPUTATIONAL MECHANICS
2018, VOL. 27, NO. 2, 143–162
https://doi.org/10.1080/17797179.2018.1484203

Taylor & Francis
Taylor & Francis Group



# Updated Lagrangian formulations of two hexahedral elements with rotational DOFs

Wajdi Zouari[a], Fodil Hammadi[b], Mustapha Assarar[a] and Rezak Ayad[a]

[a]Laboratory of Engineering and Material Sciences (LISM, EA 4695), University of Reims Champagne-Ardenne, Troyes, France; [b]Laboratory of Mechanics, Modeling and Experimentation L2MEUniversity of Bechar, Bechar, Algeria

**ABSTRACT**

Updated Lagrangian formulations of two eight-node hexahedral solid elements with rotational degrees of freedom (DOFs) are developed to analyse geometrically nonlinear large deflection problems. These two elements are based on the so-called Space Fibre Rotation (SFR) concept that considers fictive small rotations of a nodal fibre within the element to enrich the displacement vector approximation of low-order finite elements. The validity and efficiency of the proposed formulations are demonstrated by solving several nonlinear large deflection benchmarks and the obtained results show a much better accuracy than those based on the total Lagrangian approach.

**ARTICLE HISTORY**
Received 27 October 2017
Accepted 31 May 2018

**KEYWORDS**
Large deflection problems; 3D hexahedral element; rotational DOFs; updated Lagrangian scheme

## 1. Introduction

Full three-dimensional (3D) finite element numerical modelling of thin and moderately thick structures involving nonlinear geometric and material effects becomes nowadays more attractive than the classical surface modelling thanks to the advent of more powerful computing tools. It is for instance the case of sheet metal forming analysis for which classical shell elements become inaccurate when bulk deformation appears and accordingly 3D solid and solid-shell elements are more suited for this type of analysis (Mackerle, 2006; Parente, Fontes Valente, Natal Jorge, & Cardoso, 2006; Salahouelhadj, Abed-Meraim, Chalal, & Balan, 2012). Another nonlinear example concerns extrusion and injection moulding simulations in the plastic industry for which it is important to analyse 3D effects across the thickness that can not be captured by classical shell elements (Ilinca & H´Etu, 2002).

The use of standard low-order solid elements in linear and nonlinear analyses requires the enhancement of their formulations that suffer from many numerical locking pathologies leading to inaccurate and unreliable results. Within this context, several methods have been proposed for years

**CONTACT** Wajdi Zouari wajdi.zouari@univ-reims.fr

to improve the response of first-order solid elements. For example, reduced or selectively reduced integration procedures have been used to improve the computational effectiveness of low-order solid elements and prevent the volumetric locking for incompressible materials (Papoulia, 1999; Reese, 2005).

However, these techniques are known to introduce spurious deformation modes that need stabilisation procedures (Belytschko & Bindeman, 1993). Besides, some authors have considered other techniques like the method of incompatible modes or more generally the enhanced assumed strain (EAS) method to alleviate several types of locking present within standard low-order solid elements (Klinkel & Wagner, 1997; Rj, Natal Jorge, Fontes Valente, & Cesar De Sa, 2003; Simo, Armero, & Taylor, 1993; Slavkovic, Zivkovic, & Kojic, 1994). Based on these advanced methods, a consequent research effort has been made during the last 20 years to develop the so-called solid-shell elements which constitute an interesting compromise between shell and full solid elements (see e.g. Abed-Meraim & Combescure, 2009; Fontes Valente, Alves de Sousa, & Natal Jorge, 2004; Hauptmann & Schweizerhof, 1998; Klinkel, Gruttmann, & Wagner, 2006; Mostafa, Sivaselvan, & Felippa, 2013; Schwarze & Reese, 2011; Sze, Chan, & Pian, 2002, among others). In addition to that, 3D solid elements with rotational DOFs have been also proposed to solve linear elastic problems (Ayad, Zouari, Meftah, Ben Zineb, & Benjeddou, 2013; Meftah, Ayad, & Hecini, 2013; Sze & Ghali, 1993; Yunus, Pawlak, & Cook, 1991). In the work by Yunus et al. (1991), the eight-node hexahedral element HEX8R is obtained by transforming the mid-side displacement DOFs of the classical 20-node hexahedral element into corner nodal translations and rotations based on the concept of vertex rotations put forward by Allman (1984). It has been reported in Yunus et al. (1991) that the added rotational nodal variables improve considerably the accuracy of the standard eight-node hexahedral element. In the paper by Ayad et al. (2013), two eight-node hexahedral elements with rotational DOFs, named SFR8 and SFR8I, have been formulated. They are based on the so-called Space Fibre Rotation (SFR) concept introduced by Ayad (2002). This concept supposes fictive small rotations of a nodal fibre within the finite element that enhances the displacement vector approximation of low-order elements. It is important to note that the nodal rotations based on the SFR concept have no physical meaning but this latter concept has the merit to propose a more concise and direct formulation when compared to previous works dealing with drilling rotations like that of Allman (1984). The hexahedral element SFR8I is a nonconforming element because three internal (element-wise) parameters are introduced to avoid the Poisson's ratio locking in bending dominated problems.

To solve nonlinear geometric problems, the formulations of many enhanced solid and solid-shell elements have been extended based on the total Lagrangian description, the updated Lagrangian approach or the co-rotational description (Abed-Meraim & Combescure, 2009; Fontes Valente et al., 2004; Hauptmann & Schweizerhof, 1998; Klinkel & Wagner, 1997; Li, Peng, & Li, 2011; Mostafa et al., 2013; Sze et al., 2002; Wang, Chalal, & Abed-Meraim, 2017). To the authors best knowledge, only a few works, among them the recent paper by Meftah, Zouari, Sedira, and Ayad (2016), have been interested in extending solid elements with rotational DOFs to account for geometrically nonlinear problems. In this latter contribution (Meftah et al., 2016), the total Lagrangian formulations of the above mentioned SFR concept-based hexahedral elements (SFR8 and SFR8I) have been presented. Contrary to nonlinear shell elements based on the total Lagrangian scheme, Meftah et al. (2016) have not considered finite rotation kinematics because the added nodal rotations based on the SFR concept are first moderate and second have no physical meaning. It has been shown in Meftah et al. (2016) that SFR8 and SFR8I enhance the accuracy of the standard eight-node hexahedral element as in linear elastic problems. However, the response of the conforming element SFR8 has been found too stiff and far out the reference solutions. The nonconforming element SFR8I presented more accurate results than SFR8 but remains relatively stiff in some shell problems.

In this paper, we adopt an updated Lagrangian framework to describe large displacement and small strain kinematics and evaluate its impact on the SFR8 and SFR8I responses. This choice is motivated by two main reasons: firstly, the fact that the added nodal rotations based on the SFR concept are small (or moderate) which implies that an updated Lagrangian description would be more convenient than the total Lagrangian scheme adopted in Meftah et al. (2016) and secondly, the interesting results of the SFR concept-based membrane quadrilateral elements (PFR4 and PFR4I) in nonlinear geometric plane problems, under an updated Lagrangian description, recently reported by Zouari, Hammadi, and Ayad (2016).

The outline of the paper is as follows. Section 2 develops the variational formulation of the nonlinear geometric problem considering an updated Lagrangian description. In Section 3, we present the nonlinear formulations of the SFR concept hexahedral elements SFR8 and SFR8I using the updated Lagrangian framework. Section 4 deals with an evaluation of SFR8 and SFR8I responses through a set of nonlinear large deflection benchmarks.

## 2. Small strain updated Lagrangian formulation

The updated Lagrangian formulation presented in this section follows a similar description given by Zouari et al. (2016), but for completeness it is also briefly reported here.

We consider a deformable body undergoing large displacements as shown in Figure 1. Suppose that the total load applied to this body is applied in several increments so that the body occupies intermediate configurations before converging to the final configuration $C_f$. Consider the loading interval $[t_n, t_{n+1}]$ and denote with the indexes $n$ and $n+1$ all quantities at $t_n$ and $t_{n+1}$, respectively. We assume that the body is in equilibrium at $t = t_n$ and hence the configuration $C_n$ is known. In the updated Lagrangian formulation, the last known deformed configuration $C_n$ is chosen as the reference configuration $C_R$ to describe the body motion (Figure 1). An increment of the external load leads to an increment of the displacement vector between the configurations $C_n$ and $C_{n+1}$. We denote by $C_{n+1}^{(k)}$ the last known configuration between $C_n$ and $C_{n+1}$ that does not verify the body equilibrium. A correction of the displacement vector $d\Delta^{-}u$ should be determined to reach the next configuration $C_{n+1}^{(k+1)}$. The weak form of the equilibrium at configuration $C_1 \equiv C_{n+1}^{(k)}$ reads:

$$W = \int_{{}^nV} {}_n^{n+1}S_{ij}^{(k)}\,\delta({}_n^{n+1}E_{ij}^{(k)})\,d^nV - \underbrace{\left[\int_{{}^nS} {}_n^{n+1}T_i\,\delta u_i\,d^nS + \int_{{}^nV} {}_n^{n+1}f_i^v\,\delta u_i\,d^nV\right]}_{{}_n^{n+1}W_{ext}} \tag{1}$$

where ${}_n^{n+1}\underline{T}$ and ${}_n^{n+1}\underline{f}^v$ are, respectively, the boundary traction forces and the body forces applied to $C_{n+1}$ and referred to the reference configuration $C_n$, ${}_n^{n+1}\underline{\underline{S}}^{(k)}$ and ${}_n^{n+1}\underline{\underline{E}}^{(k)}$ are, respectively, the second Piola–Kirchoff stress tensor and the Green–Lagrange strain tensor of the configuration $C_1$ referred to $C_n$, and ${}_n^{n+1}W_{ext}$ denotes the virtual work done by the external loads.

To simplify, the following notation is adopted:

$${}_n^{n+1}S_{ij}^{(k)} = {}_n^1S_{ij} \quad ; \quad {}_n^{n+1}E_{ij}^{(k)} = {}_n^1E_{ij} \quad ; \quad \Delta^{-}u^{(k)} = \Delta^{-}u \tag{2}$$

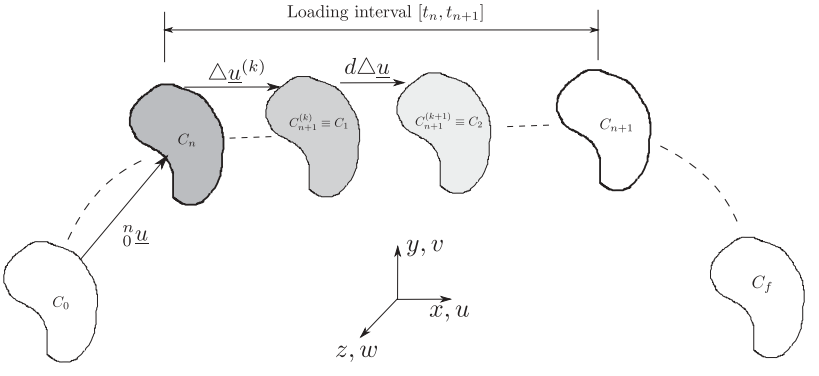


Figure 1. Reference and deformed configurations of a 3D elastic body.

which leads to a simplified expression of the weak form (1):

$$W = \underbrace{\int_{{}^{n}V} {}_{n}^{1}S_{ij}\,\delta({}_{n}^{1}E_{ij})\,d^{n}V}_{{}_{n}^{1}W_{int}} - {}_{n}^{n+1}W_{ext} \tag{3}$$

By remarking that

$${}_{n}^{1}E_{ij} = {}_{n}^{n}E_{ij} + \Delta_n E_{ij} \quad \text{and} \quad {}_{n}^{1}S_{ij} = {}_{n}^{n}S_{ij} + \Delta_n S_{ij} \tag{4}$$

the internal virtual work is rewritten as:

$${}_{n}^{1}W_{int} = \int_{{}^{n}V} {}_{n}^{1}S_{ij}\,\delta(\Delta_n E_{ij})\,d^{n}V \tag{5}$$

The increment of the Green–Lagrange strain tensor $\Delta_n \underline{\underline{E}}$ between $C_n$ and $C_1$ can be decomposed into linear $\Delta_n \underline{\underline{E}}^{lin}$ and nonlinear $\Delta_n \underline{\underline{E}}^{nl}$ strain tensors in terms of the displacement vector $\Delta \underline{u}$:

$$\begin{aligned}\Delta_n E_{ij} &= \Delta_n E_{ij}^{lin} + \Delta_n E_{ij}^{nl} \quad ; \quad \Delta_n E_{ij}^{lin} = \frac{1}{2}\left(\frac{\partial \Delta u_i}{\partial x_j} + \frac{\partial \Delta u_j}{\partial x_i}\right) \quad ; \quad \Delta_n E_{ij}^{nl} \\ &= \frac{1}{2}\left(\frac{\partial \Delta u_k}{\partial x_i} \cdot \frac{\partial \Delta u_k}{\partial x_j}\right)\end{aligned} \tag{6}$$

where $x_i$, $i$ = 1,2,3 are the Cartesian coordinates of the reference configuration $C_n$.

The use of Equations (5) and (6) into Equation (3) results in the following expression of the weak form of equilibrium at $C_1$:

$$W = \underbrace{\int_{{}^{n}V} {}_{n}^{1}S_{ij}\left(\delta(\Delta_n E_{ij}^{lin}) + \delta(\Delta_n E_{ij}^{nl})\right) d^{n}V}_{{}_{n}^{1}W_{int}} - {}_{n}^{n+1}W_{ext} \tag{7}$$

The solution of Equation (7) can be obtained by the finite element method. This will be developed in the next section by formulating two eight-node hexahedral solid elements with rotational DOFs based on the SFR concept introduced by Ayad (2002).

## 3. Finite element approximation

### 3.1 *Updated Lagrangian formulation of the conforming element SFR8*

In this subsection, we develop the updated Lagrangian formulation of the conforming hexahedral element SFR8. We start by choosing one point $q$ of the standard eight-node hexahedral element as depicted in Figure 2. The SFR concept supposes fictive small rotations, represented by the rotation vector $\underline{\theta}_i$, of the nodal fibre $\underline{iq}$ around the node $i$ (Figure 2(a)). These rotations result in an additional vector $\underline{\theta}_i \wedge \underline{iq}$ which enhances the classical approximation of the displacement vector of $q$ (Ayad, 2002; Ayad et al., 2013):

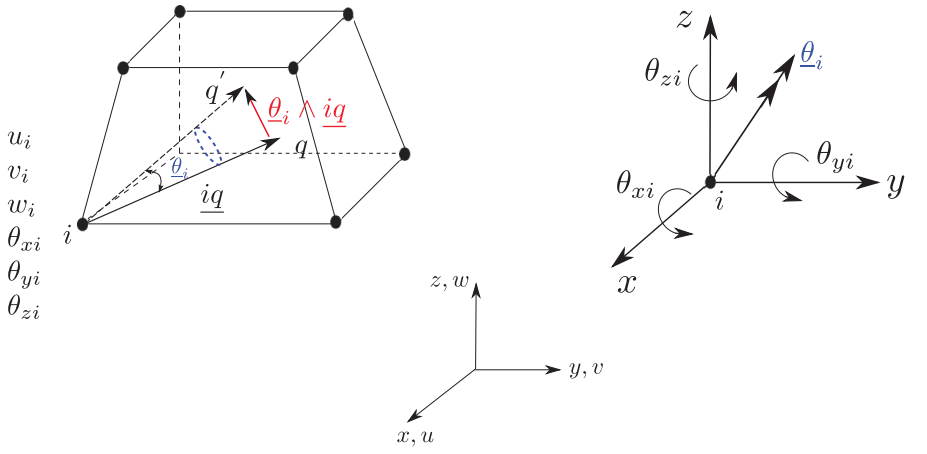


**Figure 2.** The SFR concept. (a) Fictive small rotations of the nodal fibre $\underline{iq}$ around the node $i$ inducing an additional displacement vector $\underline{\theta}_i \wedge \underline{iq}$. (b) The rotation vector $\underline{\theta_i}$ of the nodal fibre $\underline{iq}$.

$$\underline{u}_q(\xi,\eta,\zeta) = \sum_{i=1}^{8} N_i(\xi,\eta,\zeta)\left(\underline{u_i} + \underline{\theta_i} \wedge \underline{iq}\right) \Rightarrow$$
$$\left\{\begin{array}{c} u \\ v \\ w \end{array}\right\} = \sum_{i=1}^{8} N_i(\xi,\eta,\zeta) \left\{\begin{array}{l} u_i + (z-z_i)\theta_{yi} - (y-y_i)\theta_{zi} \\ v_i + (x-x_i)\theta_{zi} - (z-z_i)\theta_{xi} \\ w_i + (y-y_i)\theta_{xi} - (x-x_i)\theta_{yi} \end{array}\right\} \tag{8}$$

$N_i(\xi,\eta,\zeta)$ are the classical trilinear Lagrange interpolation functions associated with the eight-node hexahedral element, $\{u_i\} = \{u_i\, v_i\, w_i\}^T$ is the vector of nodal displacements and $\{\theta_i\} = \{\theta_{xi}\, \theta_{yi}\, \theta_{zi}\}^T$ (Figure 2(b)) is the vector of nodal fictive rotations.

As previously mentioned in the introduction, it is important to note that the small rotations of the nodal fibre $\underline{iq}$ around the node $i$ have no physical meaning from mechanics point of view.

The approximations (8) can be rewritten in a matrix form as:

$$\left\{\begin{array}{c} u \\ v \\ w \end{array}\right\} = [N]\{u_n^e\} \quad ; \quad [N] = \left[\begin{array}{c} \{N_u\}^T \\ \{N_v\}^T \\ \{N_w\}^T \end{array}\right] = \left[\begin{array}{ccc} & \{N_{ui}\}^T & \\ \cdots & \{N_{vi}\}^T & \cdots\ i = 1,8 \\ & \{N_{wi}\}^T & \end{array}\right] \tag{9}$$

where

$$\begin{array}{lcccccccc} \{N_{ui}\} & = & \{ & N_i & 0 & 0 & 0 & N_i(z-z_i) & -N_i(y-y_i) & \}^T \\ \{N_{vi}\} & = & \{ & 0 & N_i & 0 & -N_i(z-z_i) & 0 & N_i(x-x_i) & \}^T \\ \{N_{wi}\} & = & \{ & 0 & 0 & N_i & N_i(y-y_i) & -N_i(x-x_i) & 0 & \}^T \end{array} \tag{10}$$

and $\{u_n^e\} = \{\cdots \mid u_i\, v_i\, w_i \vdots \theta_{xi}\, \theta_{yi}\, \theta_{zi} \mid \cdots i = 1,8\}^T$ is the elementary nodal DOFs vector containing the nodal displacements and fictive rotations.

We introduce at this stage the following notation

$$\Delta u = \Delta u_1, \quad \Delta v = \Delta u_2, \quad \Delta w = \Delta u_3, \quad x = x_1, \quad y = x_2, \quad z = x_3 \tag{11}$$

At the element level, the internal virtual work ${}^1_nW_{int}$ is rewritten in the following matrix form:

$${}^1_nW_{int} = \int_{{}^nV} (\{\delta\Delta_n E^{lin}\}^T + \{\delta\Delta_n E^{nl}\}^T)\{{}^1_nS\}\, d^nV \tag{12}$$

Using Equation (6) and the approximations (9), it is possible to show that $\{\delta\Delta_n E^{lin}\}$ and $\{\delta\Delta_n E^{nl}\}$ are related to $\{\delta\Delta u_n^e\}$ through two matrices $[B_L]$ and $[B_{NL}]$, respectively, as follows:

$$\{\delta\Delta_n E^{lin}\} = [B_L]\{\delta\Delta u_n^e\}; \{\delta\Delta_n E^{nl}\} = [B_{NL}]\{\delta\Delta u_n^e\} \tag{13}$$

where

$$\underbrace{[B_L]}_{(6\times 48)} = \begin{bmatrix} N_{i,x} & 0 & 0 & 0 & N_{i,x}(z-z_i) & -N_{i,x}(y-y_i) & \\ 0 & N_{i,y} & 0 & -N_{i,y}(z-z_i) & 0 & N_{i,y}(x-x_i) & \\ 0 & 0 & N_{i,z} & N_{i,z}(y-y_i) & -N_{i,z}(x-x_i) & 0 & \\ \cdots\ N_{i,y} & N_{i,x} & 0 & -N_{i,x}(z-z_i) & N_{i,y}(z-z_i) & N_{i,x}(x-x_i) - & \cdots i = 1,8 \\ & & & & & N_{i,y}(y-y_i) & \\ N_{i,z} & 0 & N_{i,x} & N_{i,x}(y-y_i) & N_{i,z}(z-z_i) - & -N_{i,z}(y-y_i) & \\ & & & & N_{i,x}(x-x_i) & & \\ 0 & N_{i,z} & N_{i,y} & N_{i,y}(y-y_i) - & -N_{i,y}(x-x_i) & N_{i,z}(x-x_i) & \\ & & & N_{i,z}(z-z_i) & & & \end{bmatrix}, \tag{14}$$

$$\underbrace{[B_{NL}]}_{(6\times 48)} = [B_\phi][B_\sigma],\ \underbrace{[B_\phi]}_{(6\times 9)}$$

$$= \begin{bmatrix} \Delta u_{,x} & 0 & 0 & \Delta v_{,x} & 0 & 0 & \Delta w_{,x} & 0 & 0 \\ 0 & \Delta u_{,y} & 0 & 0 & \Delta v_{,y} & 0 & 0 & \Delta w_{,y} & 0 \\ 0 & 0 & \Delta u_{,z} & 0 & 0 & \Delta v_{,z} & 0 & 0 & \Delta w_{,z} \\ \Delta u_{,y} & \Delta u_{,x} & 0 & \Delta v_{,y} & \Delta v_{,x} & 0 & \Delta w_{,y} & \Delta w_{,x} & 0 \\ \Delta u_{,z} & 0 & \Delta u_{,x} & \Delta v_{,z} & 0 & \Delta v_{,x} & \Delta w_{,z} & 0 & \Delta w_{,x} \\ 0 & \Delta u_{,z} & \Delta u_{,y} & 0 & \Delta v_{,z} & \Delta v_{,y} & 0 & \Delta w_{,z} & \Delta w_{,y} \end{bmatrix}, \tag{15}$$

$$\underbrace{[B_\sigma]}_{(9\times 48)} = \begin{bmatrix} & \{N_{ui,x}\}^T & \\ & \{N_{ui,y}\}^T & \\ & \{N_{ui,z}\}^T & \\ & \{N_{vi,x}\}^T & \\ \cdots & \{N_{vi,y}\}^T & \cdots\, i = 1,8 \\ & \{N_{vi,z}\}^T & \\ & \{N_{wi,x}\}^T & \\ & \{N_{wi,y}\}^T & \\ & \{N_{wi,z}\}^T & \end{bmatrix} \tag{16}$$

and

$$N_{i,\alpha} = \frac{\partial N_i}{\partial \alpha}, \quad \{N_{ui,\alpha}\} = \frac{\partial \{N_{ui}\}}{\partial \alpha}, \quad \alpha = x, y, z$$

Accordingly, the residual vector of the conforming element SFR8 is given by:

$$\{R^e\} = \{{}^{n+1}_{n}F^e_{ext}\} - \{{}^{1}_{n}F^e_{int}\} \quad ; \quad \{{}^{1}_{n}F^e_{int}\} = \int_{{}^nV} ([B_L]^T + [B_{NL}]^T)\{{}^{1}_{n}S\}\, d^nV \tag{17}$$

The elementary tangent stiffness matrix of SFR8 is found by performing a variation of the internal virtual work:

$$\begin{aligned} &{}^{1}_{n}W_{int} = \int_{{}^nV} \{\delta\Delta_n E\}^T \{{}^{1}_{n}S\}\, d^nV \quad \Rightarrow \\ &dW_{int} = \int_{{}^nV} \{\delta\Delta_n E\}^T \{d\Delta S\}\, d^nV + \int_{{}^nV} \{d\delta\Delta_n E^{nl}\}^T \{{}^{1}_{n}S\}\, d^nV \end{aligned} \tag{18}$$

By remarking that $\{d\Delta S\} = [C]\{d\Delta E\}$ where $[C]$ is the (6 × 6)-sized elasticity matrix, the first term of $dW_{int}$ gives the linear and nonlinear stiffness matrices of SFR8:

$$[K^e_L] = \int_{{}^nV} [B_L]^T [C][B_L]\, d^nV \tag{19}$$

$$[K^e_{NL}] = \int_{{}^nV} ([B_L]^T [C][B_{NL}] + [B_{NL}]^T [C][B_L] + [B_{NL}]^T [C][B_{NL}])\, d^nV \tag{20}$$

The geometric stiffness matrix is obtained from the second term of $dW_{int}$ as follows:

$$[K^e_{geom}] = \int_{{}^nV} [B_\sigma]^T [{}^{1}_{n}\bar{S}][B_\sigma]\, d^nV \quad \text{with} \quad [{}^{1}_{n}\bar{S}] = \begin{bmatrix} [{}^{1}_{n}S] & 0 & 0 \\ 0 & [{}^{1}_{n}S] & 0 \\ 0 & 0 & [{}^{1}_{n}S] \end{bmatrix} \tag{21}$$

and

$$[{}^{1}_{n}S] = \begin{bmatrix} {}^{1}_{n}S_{xx} & {}^{1}_{n}S_{xy} & {}^{1}_{n}S_{xz} \\ {}^{1}_{n}S_{xy} & {}^{1}_{n}S_{yy} & {}^{1}_{n}S_{yz} \\ {}^{1}_{n}S_{xz} & {}^{1}_{n}S_{yz} & {}^{1}_{n}S_{zz} \end{bmatrix}$$

Finally, the following finite element model is solved to determine the correction $\{d\Delta u^e_n\}$ between $C_1$ and $C_2$:

$$(\underbrace{[K^e_L] + [K^e_{NL}] + [K^e_{geom}]}_{[K^e_T]})\{d\Delta u^e_n\} = \{R^e\} \tag{22}$$

where $[K^e_T]$ is the elementary tangent stiffness matrix of SFR8.

### 3.2. *Updated Lagrangian formulation of the nonconforming element SFR8I*

We introduce three incompatible displacement modes $a_u$, $a_v$ and $a_w$ in the natural space of SFR8 to avoid the Poisson's ratio locking as explained in Ayad et al. (2013; Yunus et al., 1991). The natural space extra modes are given as follows:

$$\begin{cases} u^a = (1-\xi^2)\, a_u \\ v^a = (1-\eta^2)\, a_v \\ w^a = (1-\zeta^2)\, a_w \end{cases} \tag{23}$$

In this case, we obtain an enhanced Green–Lagrange strain vector:

$$\{E\} = \{E^u\} + \{E^a\}, \quad \{E^a\} = [M^a]\{a\} \tag{24}$$

where $\{E^u\}$ and $\{E^a\}$ are, respectively, the conforming and nonconforming strain vectors, $\{a\}$ is the vector of incompatible modes and $[M^a]$ the matrix relating $\{E^a\}$ to $\{a\}$ (see Ayad et al., 2013 for more details).

After introducing the enhanced strain vector in the equilibrium weak form (3) at the element level, we obtain the following system of equations:

$$\begin{bmatrix} [K^e_L] + [K^e_{NL}] + [K^e_{geom}] & [K^e_{ua}] \\ [K^e_{au}] & [K^e_{aa}] \end{bmatrix} \begin{Bmatrix} \{d\Delta u^e_n\} \\ \{d\Delta a\} \end{Bmatrix} = \begin{Bmatrix} \{{}^{n+1}_{n}F^{\,e}_{ext}\} - \int_{{}^{n}V} ([B_L]^T + [B_{NL}]^T)\{{}^{1}_{n}S\}\, d^nV \\ -\int_{{}^{n}V} [M^a]^T \{{}^{1}_{n}S\}\, d^nV \end{Bmatrix} \tag{25}$$

where

$$\begin{aligned}[K^e_{ua}] &= \int_{^nV}([B_L]^T + [B_{NL}]^T)[C][M^a]\,d^nV, \quad [K^e_{au}] = [K^e_{ua}]^T,\\ [K^e_{aa}] &= \int_{^nV}[M^a]^T[C][M^a]\,d^nV\end{aligned} \tag{26}$$

The vector of internal variables $\{d\Delta a\}$ can be eliminated at the element level by using a static condensation. We obtain

$$\{d\Delta a\} = -[K^e_{aa}]^{-1}\left([K^e_{au}]\{d\Delta u^e_n\} + \int_{^nV}[M^a]^T\{{}^1_nS\}\,d^nV\right) \tag{27}$$

Finally, the following system of equations should be solved to determine the correction $\{d\Delta u^e_n\}$ for the nonconforming element SFR8I:

$$[\bar{K}^e_T]\{d\Delta u^e_n\} = \{\bar{R}^e\} \tag{28}$$

with

$$[\bar{K}^e_T] = [K^e_L] + [K^e_{NL}] + [K^e_{geom}] - [K^e_{ua}][K^e_{aa}]^{-1}[K^e_{au}] \tag{29}$$

$$\begin{aligned}\{\bar{R}^e\} = \{{}^{n+1}_nF^e_{ext}\} - \int_{^nV}([B_L]^T + [B_{NL}]^T)\{{}^1_nS\}\,d^nV\\ + [K^e_{ua}][K^e_{aa}]^{-1}\int_{^nV}[M^a]^T\{{}^1_nS\}\,d^nV\end{aligned} \tag{30}$$

$[\bar{K}^e_T]$ and $\{\bar{R}^e\}$ are the elementary tangent stiffness matrix and the residual vector of SFR8I, respectively.

It is worthy to note that a $2 \times 2 \times 2$ Gauss points numerical integration scheme was chosen to calculate all terms of SFR8 and SFR8I formulations. The tangent stiffness matrices of these two elements exhibit 12 spurious zero-energy modes which are controlled by the same stabilisation technique as in Ayad et al. (2013).

## 4. Numerical validation

This section is devoted to assess the capability and accuracy of the above-proposed formulations in some popular nonlinear benchmark problems. The presented results are obtained from the finite element code ABAQUS Standard after introducing SFR8 and SFR8I, under the updated Lagrangian description, as user elements (ABAQUS, 2016). The results of the SFR concept-based hexahedral elements are compared with those based on the total Lagrangian approach (Meftah et al., 2016) and some advanced solid and solid-shell elements from the literature. To simplify the presentation of the obtained results, SFR8 and SFR8I based on the total and the updated Lagrangian frameworks are designated by SFR8-TL, SFR8I-TL and SFR8-UL, SFR8I-UL, respectively. To carry out finite element calculations with the SFR concept-based elements, constraints on the rotational DOFs are prescribed in addition to the classical displacement ones (see Ayad et al., 2013 for more details).

For all the following numerical examples, the total numbers of increments and iterations required to reach the ultimate solutions were found to be equivalent to those reported in Meftah et al. (2016).

### 4.1. *Clamped square plate subjected to a uniform load*

A thin clamped square plate is subjected to a uniformly distributed load $q = 20$ as shown in Figure 3. Owing to symmetry, only one-quarter of the square plate is analysed with $4 \times 4 \times 1$ hexahedral elements (Figure 4). We show in Figure 4 the load–central deflection curves of SFR8 and SFR8I

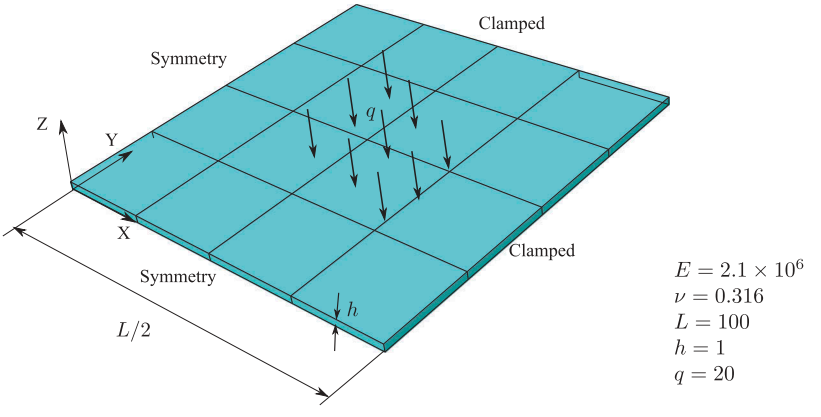


Figure 3. One quarter of the clamped square plate modelled with $4 \times 4 \times 1$ hexahedral elements.

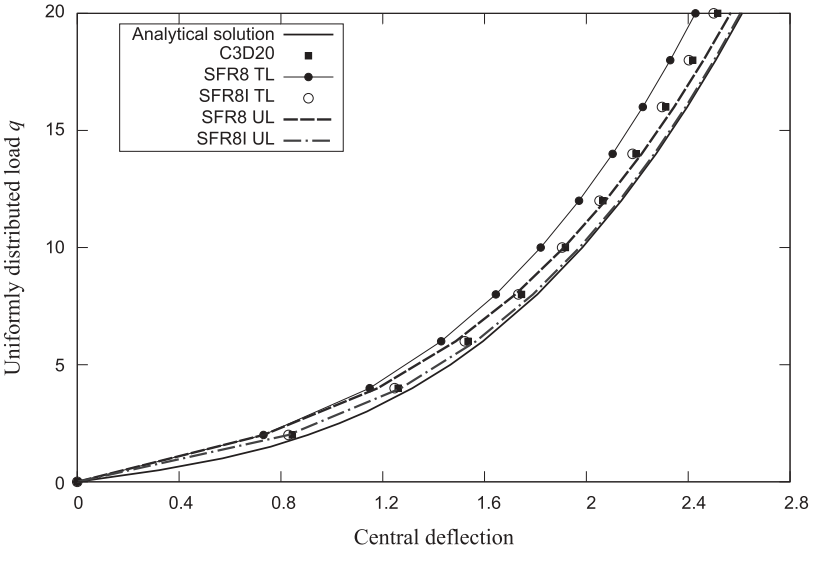


Figure 4. Load–central deflection curve of the clamped square plate.

compared with the analytical solution by Chia (1980) and C3D20 (the classical 20-node hexahedral element of ABAQUS with an exact numerical integration scheme).

We remark that the obtained results agree globally well with the analytic solution by Chia (1980). For small values of the central deflection (lower than 1.2), the total and updated Lagrangian schemes give approximately the same results with SFR8 and SFR8I. However, for higher values, a notable difference between the two formulations is observed and the updated Lagrangian description gives more accurate results than the total Lagrangian scheme.

### 4.2. *Clamped circular plate subjected to a concentrated load*

We consider in this second example the clamped circular plate of Figure 5 subjected at its centre to a concentrated load $F$ that is increased up to $F^{max} = 10^6$. Thanks to symmetry, only one-quarter of the circular plate is modelled with 12 hexahedral elements (Figure 5). The load–central deflection curves of SFR8 and SFR8I, compared to C3D20 and the analytical solution by Chia (1980), are depicted in Figure 6. Globally, the same remarks as the clamped square plate (Section 4.1) hold for this second example.

### 4.3. *Pullout of an open-ended cylindrical shell*

An open-end cylindrical shell of length $L = 10.35$, radius $R = 4.953$ and constant thickness $h = 0.094$ loaded by two opposite concentrated loads is

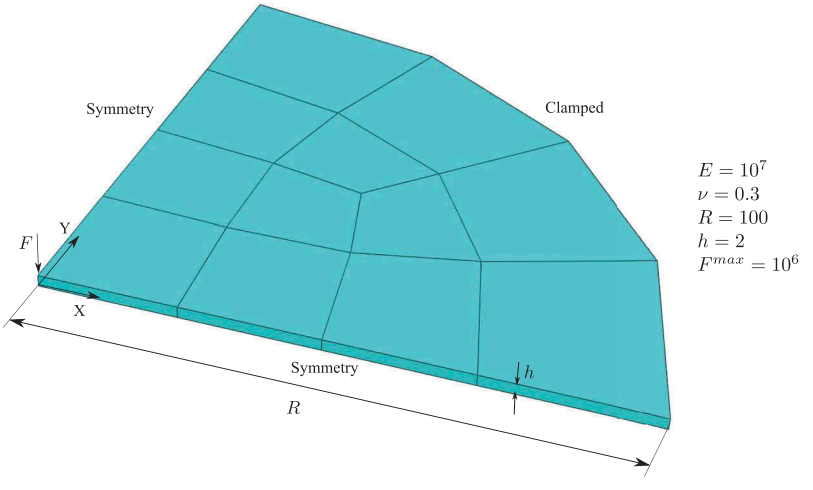


Figure 5. One quarter of the clamped circular plate modelled with 12 hexahedral elements.

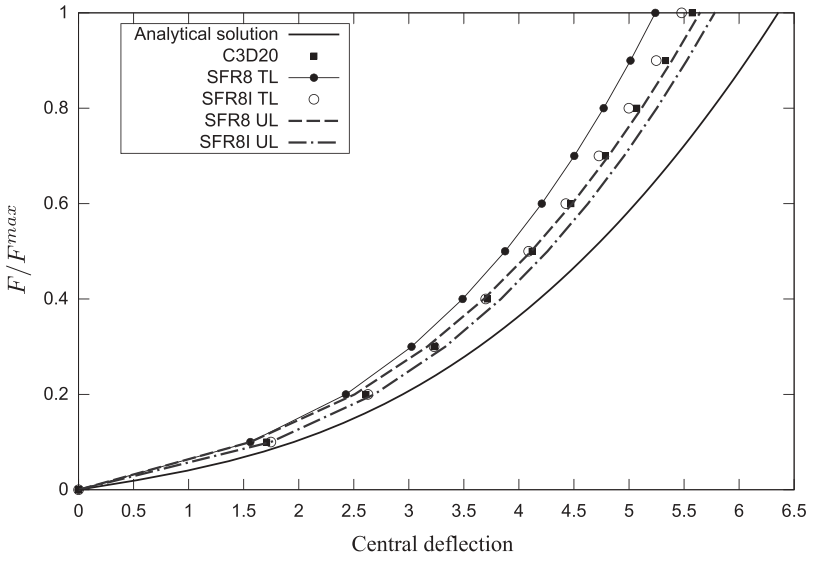


Figure 6. Load–deflection curve of the clamped circular plate.

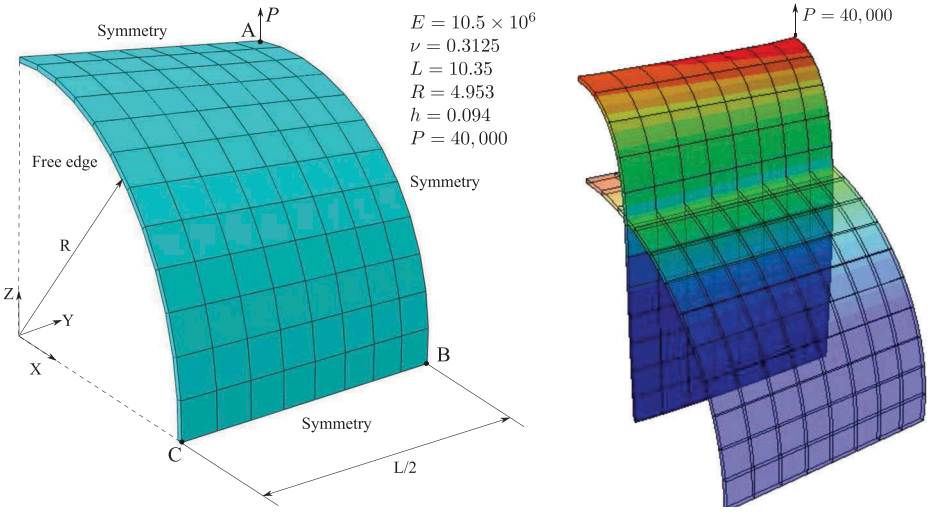


Figure 7. One-eighth of the open-end cylindrical shell modelled with 8 × 12 × 1 hexahedral elements.

considered. Owing to symmetry, only one-eighth of the cylinder is modelled with 8 × 12 × 1 hexahedral elements as depicted in Figure 7 and adopted in Fontes Valente et al. 2004 and Sze et al., 2002. The applied load is increased up to 40,000 and the displacements of points A along Z and B and C along X (Figure 7) are determined. Figure 8 shows the load–deflection curves at points A, B and C of SFR8 and SFR8I compared with the reference solutions by Sze et al. (2004), the solid-shell element HS of Sze et al. (2002) and the solid-shell element HCiS12 of Fontes

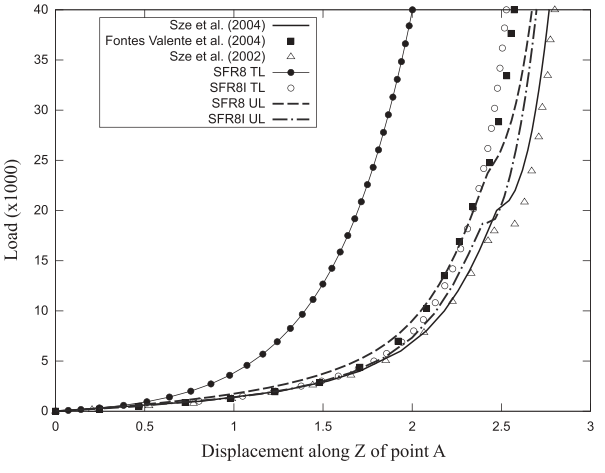


(a)

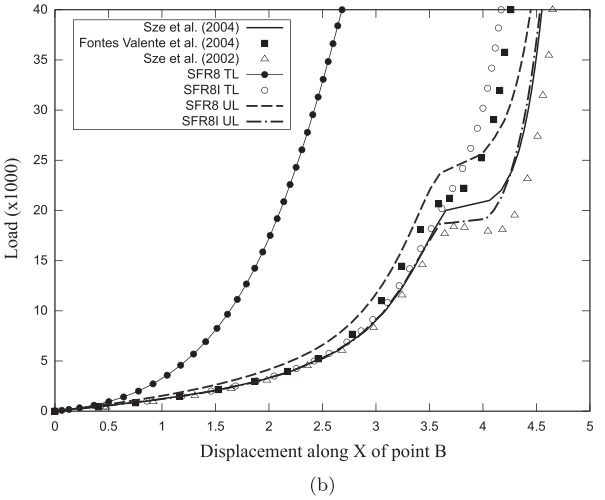


(b)

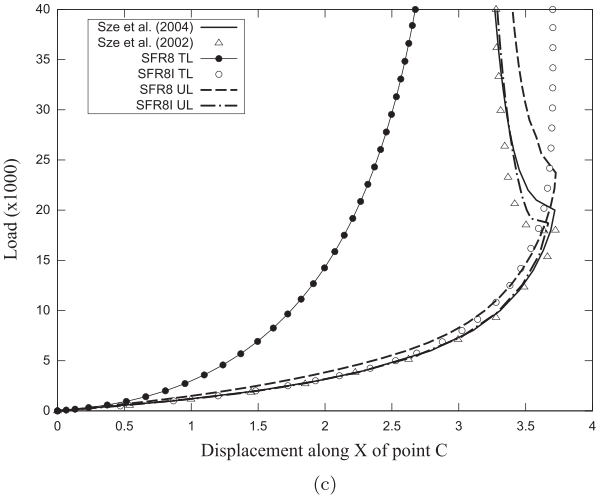


(c)

**Figure 8.** The open-end cylindrical shell. (a) Load–displacement along Z of point A curve. (b) Load–displacement along X of point B curve. (c) Load–displacement along X of point C curve.

Valente et al. (2004). It is worth noting that the results of the solid-shell element HS shown in Figure 8 are based on an updated Lagrangian scheme. Moreover, Sze et al. (2002) have reported a notable difference between the total and updated Lagrangian descriptions results.

First, we remark that the adopted updated Lagrangian description permits to largely enhance the accuracy of the conforming element SFR8 and in this case SFR8-UL results are in good agreement with the reference curves by Sze et al. (2004). Second, the updated Lagrangian scheme allows also to clearly improve the SFR8I accuracy especially to predict the slight snap-through behaviour of the cylindrical shell around $P = 20,000$.

### 4.4. *Pinching of a clamped cylinder*

A cantilever elastic cylindrical shell subjected to two opposite concentrated loads is analysed in this example. Owing to symmetry, only one-quarter of the cylinder is modelled with $16 \times 16 \times 1$ hexahedral elements as depicted in Figure 9 and considered in Fontes Valente et al. (2004). We show in Figure 10 the obtained load–deflection curves of SFR8 and SFR8I compared with the solid-shell element HCiS12 of Fontes Valente et al. (2004) and the four-node shell element of Brank, Damjanic, and Peric (1995) (taken as the reference curve).

The load–deflection curves of Figure 10 show that the too stiff behaviour of SFR8-TL is clearly enhanced by the adopted updated Lagrangian approach. The SFR8I-UL solution, which is found very close to HCiS12, also largely surpasses that of SFR8I-TL and correctly predicts the slight instability of the cylindrical shell around $F = 700$.

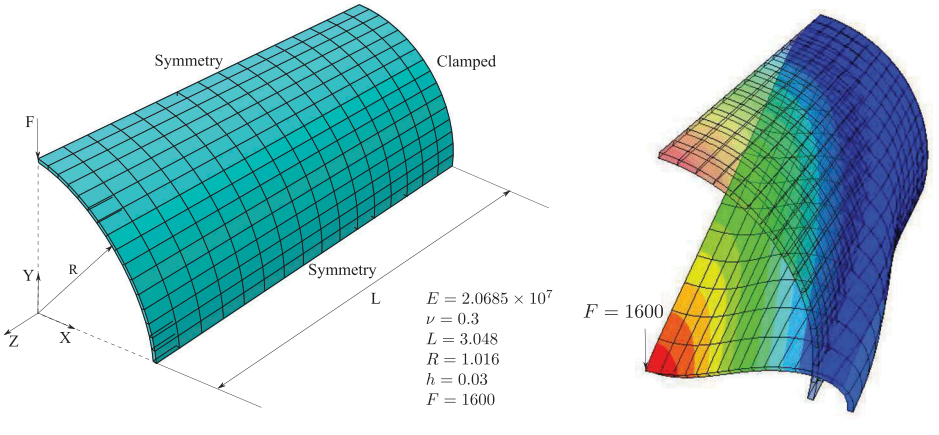


Figure 9. One-fourth of the pinched clamped cylinder modelled with $16 \times 16 \times 1$ hexahedral elements.

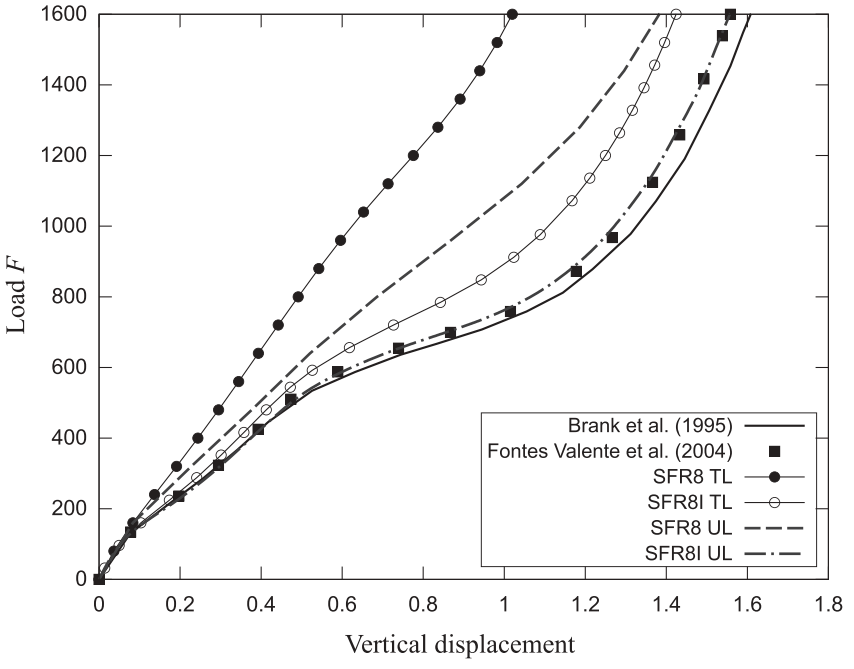


Figure 10. Load–displacement curve of the pinched cylindrical shell.

### 4.5. *Hinged cylindrical roofs subjected to central point loads*

We consider in this last assessment test two thin and thick circular cylindrical roofs subjected to central point loads as depicted in Figure 11. The longitudinal boundaries are hinged and immovable while the curved edges are completely free. Thanks to symmetry, only a quarter of each roof is modelled with $4 \times 4 \times 2$ hexahedral elements as considered in Mostafa et al. 2013 and Schwarze & Reese, 2011 (Figure 11). The use of two elements across the thickness permits to correctly represent hinged boundary conditions as explained in Mostafa et al. (2013). Due to the snapping behaviour, the arc-length method is used to solve this problem. We show in Figures 12 and 13 the load–displacement curves of SFR8 and SFR8I compared with the solid-shell element Q1TSs of Schwarze and Reese (2011), the solid-shell element of Mostafa et al. (2013) (only for the thin shell) and the reference curves by Sze et al. (2004).

We remark that SFR8 and SFR8I with the total and updated Lagrangian descriptions predict correctly the unstable snap-back and snap-through behaviours of the thin and thick cylindrical roofs. As for the previous studied benchmarks, the updated Lagrangian approach enhances in particular the response of the conforming element SFR8 whose results show better agreement with the reference curves.

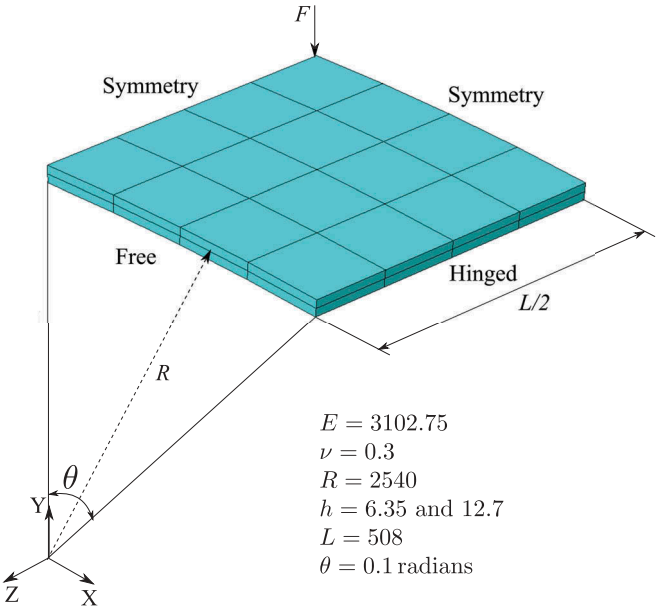


Figure 11. One-fourth of the hinged cylindrical roof modelled with 4 × 4 × 2 hexahedral elements.

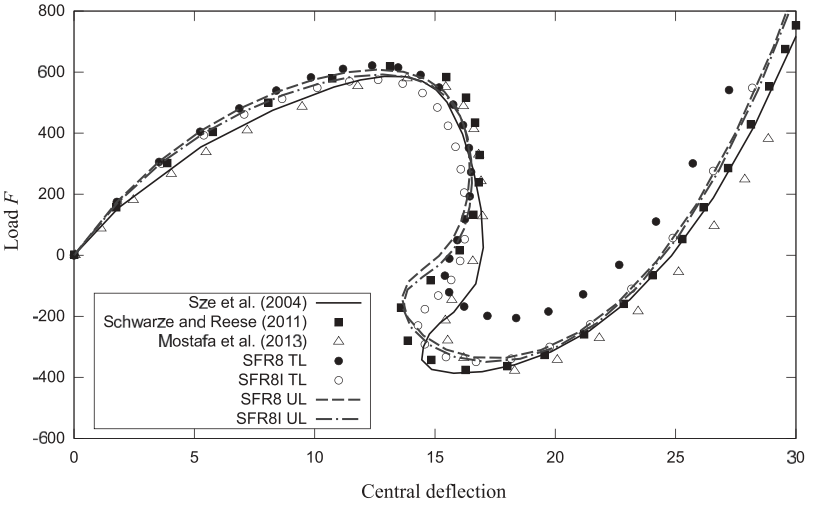


Figure 12. Load–deflection curve of the thin hinged cylindrical roof.

## 5. Conclusion

Based on the so-called SFR concept, two eight-node solid hexahedral elements with rotational DOFs, named SFR8 and SFR8I, were developed by the updated Lagrangian approach to analyse geometrically nonlinear large deflection problems. As validation tests, five plate and shell nonlinear

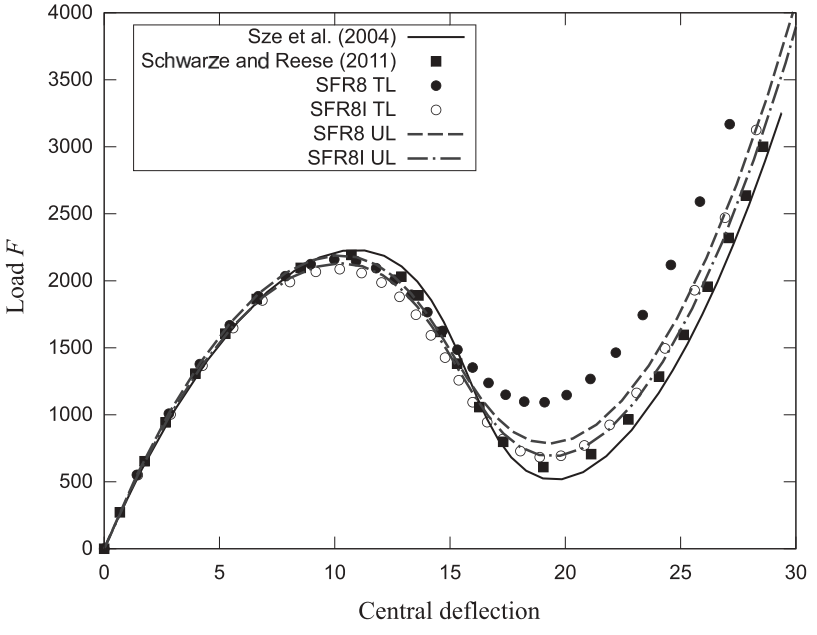


Figure 13. Load–deflection curve of the thick hinged cylindrical roof.

benchmarks were considered and the obtained results were mainly compared with those based on the total Lagrangian description. In particular, it was found that the updated Lagrangian approach significantly enhances the accuracy of the conforming element SFR8 compared with the total Lagrangian description. Besides, the relatively stiff behaviour of the non-conforming element SFR8I in some shell problems seems to be improved by the proposed updated formulation.

## Disclosure statement

No potential conflict of interest was reported by the authors.

## References

ABAQUS. (2016). Analysis user's manual. V.6, 14.

Abed-Meraim, F., & Combescure, A. (2009). An improved assumed strain solid-shell element formulation with physical stabilization for geometric non-linear applications and elastic-plastic stability analysis. *International Journal for Numerical Methods in Engineering*, *80*(13), 1640–1686.

Allman, D. J. (1984). A compatible triangular element including vertex rotations for plane elasticity analysis. *Computers and Structures*, *19*, 1–8.

Ayad, R. (2002).*Contribution to the numerical modeling of solids and structures and the non-newtonian fluids forming process. Application to packaging materials* (in French) (PhD dissertation). Habilitation to conduct researches. University of Reims.

Ayad, R., Zouari, W., Meftah, K., Ben Zineb, T., & Benjeddou, A. (2013). Enrichment of linear hexahedral finite elements using rotations of a virtual space fiber. *International Journal for Numerical Methods in Engineering*, *95*, 46–70.

Belytschko, T., & Bindeman, L. P. (1993). Assumed strain stabilization of the eight node hexahedral element. *Computer Methods in Applied Mechanics and Engineering*, *105*, 225–260.

Brank, B., Damjanic, F., & Peric, D. (1995). On implementation of a nonlinear four node shell finite element for thin multilayered elastic shells. *Computational Mechanics*, *16*(5), 341–359.

Chia, C. Y. (1980). *Nonlinear analysis of plates*. London: McGraw-Hill.

Fontes Valente, R. A., Alves de Sousa, R. J., & Natal Jorge, R. M. (2004). An enhanced strain 3D element for large deformation elastoplastic thin-shell applications. *Computational Mechanics*, *34*, :38–52.

Hauptmann, R., & Schweizerhof, K. (1998). A systematic development of solid-shell element formulations for linear and non-linear analyses employing only displacement degrees of freedom. *International Journal for Numerical Methods in Engineering*, *42*(1), 49–69.

Ilinca, F., & H´Etu, J. F. (2002). Three-dimensional finite element solution of gas-assisted injection moulding. *International Journal for Numerical Methods in Engineering*, *53*, 2003–2017.

Klinkel, S., Gruttmann, F., & Wagner, W. (2006). A robust non-linear solid shell element based on a mixed variational formulation. *Computer Methods in Applied Mechanics and Engineering*, *195*, 179–201.

Klinkel, S., & Wagner, W. (1997). A geometrical non-linear brick element based on the EAS-method. *International Journal for Numerical Methods in Engineering*, *40*(24), 4529–4545.

Li, L. M., Peng, Y. H., & Li, D. Y. (2011). A stabilized underintegrated enhanced assumed strain solid-shell element for geometrically nonlinear plate/shell analysis. *Finite Elements in Analysis and Design*, *47*(5), 511–518.

Mackerle, J. (2006). Finite element modelling and simulation of bulk material forming: A bibliography (1996–2005). *Engineering Computations*, *23*(3), 250–342.

Meftah, K., Ayad, R., & Hecini, M. (2013). A new 3D 6-node solid finite element based upon the space fibre rotation concept. *European Journal of Computational Mechanics*, *22*(1), 1–29.

Meftah, K., Zouari, W., Sedira, L., & Ayad, R. (2016). Geometric non-linear hexahedral elements with rotational DOFs. *Computational* 51. *Mechanics*, *57*, 37–53.

Mostafa, M., Sivaselvan, M. V., & Felippa, C. A. (2013). A solid-shell corotational element based on ANDES, ANS and EAS for geomet-rically nonlinear structural analysis. *International Journal for Numerical Methods in Engineering*, *95*(2), 145–180.

Papoulia, K. D. (1999). Mixed and selective reduced integration procedures in large strain hyperelastic analysis of nearly incom- pressible solids. *Computational Mechanics*, *23*(1), 63–74.

Parente, M. P. L., Fontes Valente, R. A., Natal Jorge, R. M., & Cardoso, R. P. R. (2006). Alves de Sousa RJ. Sheet metal forming simulation using EAS solid-shell finite elements. *Finite Elements in Analysis and Design*, *42*, 1137–1149.

Reese, S. (2005). On a physically stabilized one point finite element formulation for three-dimensional finite elasto-plasticity. *Computer Methods in Applied Mechanics and Engineering*, *194*, 4685–4715.

Rj, A. D. S., Natal Jorge, R. M., Fontes Valente, R. A., & Cesar de Sa, J. M. A. (2003). A new volumetric and shear locking-free 3D enhanced strain element. *Engineering Computations*, *20*, 896–925.

Salahouelhadj, A., Abed-Meraim, F., Chalal, H., & Balan, T. (2012). Application of the continuum shell finite element SHB8PS to sheet forming simulation using an extended large strain anisotropic elastic–Plastic formulation. *Archive of Applied Mechanics*, *82*(9), 1269–1290.

Schwarze, M., & Reese, S. (2011). A reduced integration solid-shell finite element based on the EAS and the ANS concept–Large deformation problems. *International Journal for Numerical Methods in Engineering*, *85*(3), 289–329.

Simo, J. C., Armero, F., & Taylor, R. L. (1993). Improved versions of assumed enhanced strain tri-linear elements for 3d finite deformation problems. *Computer Methods in Applied Mechanics and Engineering*, *110*, 359–386.

Slavkovic, R., Zivkovic, M., & Kojic, M. (1994). Enhanced 8-node three-dimensional solid and 4-node shell elements with incompatible generalized displacements. *Communications in Numerical Methods in Engineering*, *10*(9), 699–709.

Sze, K. Y., Chan, W. K., & Pian, T. H. H. (2002). An eight-node hybrid-stress solid-shell element for geometric non-linear analysis of elastic shells. *International Journal for Numerical Methods in Engineering*, *55*(7), 853–878.

Sze, K. Y., & Ghali, A. (1993). A hybrid brick element with rotational degrees of freedom. *Computational Mechanics*, *12*, 147–163.

Sze, K. Y., Liu, X. H., & Lo, S. H. (2004). Popular benchmark problems for geometric nonlinear analysis of shells. *Finite Elements in 56 Analysis and Design*, *40*(11), 1551–1569.

Wang, P., Chalal, H., & Abed-Meraim, F. (2017). Quadratic solid–Shell elements for nonlinear structural analysis and sheet metal forming simulation. *Computational Mechanics*, *59*(1), 161–186.

Yunus, S. M., Pawlak, T. P., & Cook, R. D. (1991). Solid elements with rotational degrees of freedom: Part I–Hexahedron elements. *Inter- National Journal for Numerical Methods in Engineering*, *31*, 573–592.

Zouari, W., Hammadi, F., & Ayad, R. (2016). Quadrilateral membrane finite elements with rotational DOFs for the analysis of geo- metrically linear and nonlinear plane problems. *Computers and Structures*, *173*, 139–149.